JOURNAL OF COMPUTATIONAL PHYSICS **143,** 462–483 (1998)
ARTICLE NO. CP985858

An Efficient Boundary Integral Formulation for Flow Through Fractured Porous Media

M. F. Lough, S. H. Lee, and J. Kamath

Chevron Petroleum Technology Company, P.O. Box 446, La Habra, California 90633-0446
E-mail: mfl@cobra.jpl.nasa.gov, shl@chevron.com, and jkam@chevron.com

Received April 25, 1997; revised October 1, 1997

In this paper we present a new model for flow in fractured porous media. We formulate our model in terms of a coupled system of boundary integral equations and present an efficient procedure for solving the equations using the boundary element method. In the new model, the flow in the matrix is governed by the usual Darcy law for porous media, with the fractures being treated as planar sources embedded in the matrix. The flow in an individual fracture is governed by a two-dimensional Darcy law (as in a Hele–Shaw cell), with an associated planar sink distribution. The essential feature of this approach is that the fractures are treated as special planes rather than narrow-gap voids. The error in the resulting system of equations is on the order of an intrinsic dimensionless parameter (the ratio of the fracture gap size to the scale of the volume under consideration). We also describe how we adapt the new model to compute effective grid block permeabilities. This was the principal motivation behind the development of the new model. Using effective grid block permeabilities to model flow in fractured oil and gas reservoirs is a much more efficient process than modeling the flow when every fracture is precisely represented. We present some numerical examples that illustrate the new flow model and how it is used to model flow in a reservoir.

Key Words: boundary integral formulation; effective permeability; fractured porous media.

1. INTRODUCTION

The macroscopic behavior of fluid flow in porous media is well known to be described by Darcy's law. The porous medium comprises a matrix of solid material with an included distribution of pores. The pores make up the so called void-space for the medium and, as such, they may contain and conduct fluid. If the pores form connected pathways, the material will be permeable and the manner in which the pores are connected will determine the tensorial permeability of the medium. It has been well established that the local permeability tensor is always symmetric (cf. Bear [1]).

0021-9991/98 $25.00

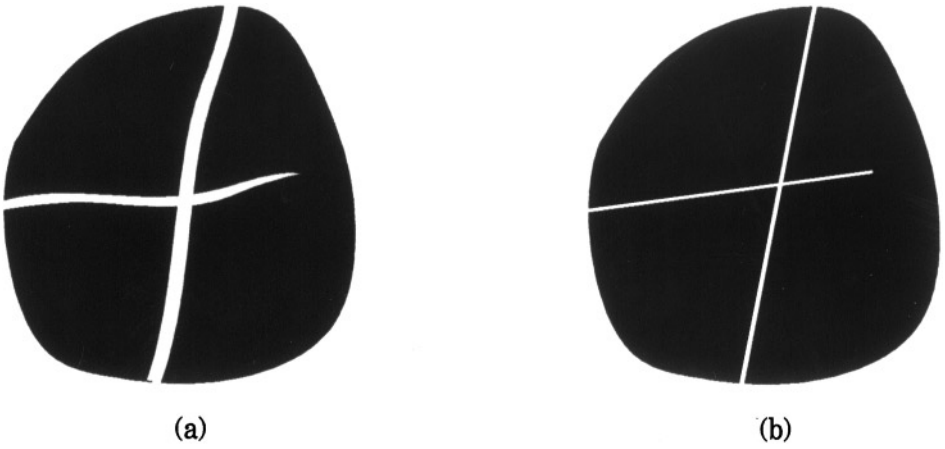

FIG. 1. A typical cross section through a region of fractured porous rock; (a) real representation of fracture shape, (b) idealized representation of fracture shape.

In many porous reservoirs, it is not unusual for the rock to become fractured at some stage in its history. This can happen in a number of ways, for example, the fractures may be caused by nearby seismic activity or through local deformation of the strata containing the porous rock. In Fig. 1a we depict a typical cross section through a region of a fractured reservoir. The matrix is represented as a shaded region separated by unshaded strips, the fractures. The effect of a single fracture is to introduce a new type of void space into the matrix. This new type of void space is very different from the void space associated with the indigenous pores. This is because it extends for a significant distance in two fairly well defined directions. These are the directions that roughly describe the planar shape of the fracture. The extent of the fracture in the third direction, the fracture gap, is usually much smaller than the fracture length or diameter, but is still typically several orders of magnitude greater than the pore size. It follows, that the presence of a single fracture will significantly impact the local permeability in the neighborhood of the fracture. Consequently, the performance and recovery rates, for fractured oil and gas reservoirs, can be expected to be significantly influenced by the interaction of the fracture system with the porous rock. Unfortunately, this type of interaction is very poorly understood at the reservoir scale. In order to be able understand this type of interaction, we need to be able to model the flow through a region like that depicted in Fig. 1a. This is certainly possible, so long as the shapes of the fractures are known. However, we usually only have information about the general properties of the fracture shape. Most often this entails information about the statistical variation of quantities such as the fracture gap, fracture length, fracture orientation and so on. To accommodate this information, fractures are idealized as planar voids inside the matrix. In Fig. 1b we depict the idealized cross section corresponding to the cross section of Fig. 1a. In each planar void the fluid flow can be modeled as being equivalent to the flow between a pair of parallel plates as in a Hele–Shaw cell (cf. Homsy [2]). This implies that the flow in an individual fracture is essentially two-dimensional.

A much more insurmountable restriction, when modeling flow in fractured reservoirs, is that there are usually too many fractures to be explicitly included in a flow model. One of the current approaches for circumventing this problem relies on ignoring the flow through the matrix rock, so that flow only takes place through connected systems of two-dimensional

fracture planes. This approach has the drawback that two points in the reservoir cannot communicate with each other unless there is a connected system of fractures joining the points. A second approach relies on representing the matrix and fracture systems as a pair of overlapping continua. Unfortunately, in this approach the permeability associated with the grid blocks in the fracture continuum is based on the assumption that the fractures are infinitely long, orthogonal, and regularly spaced. Real fracture systems do not appear to have these properties. Moreover, recent field characterization studies (cf. Chiles [3], Laubach [4], and Lorenz and Hill [5]) have shown that fracture systems are very irregular, often disconnected and may occur in swarms. To include such complex features in a flow model clearly requires a new modeling approach.

The approach we propose is to replace each fractured grid block with a grid block that has an equivalent effective, or homogenized, permeability. The effective grid block permeability should be computed so as to take into account the geometry of the actual fracture system in the grid block. In this way, the effective grid block permeability will retain information about the complexity of the fracture system that was initially contained in the grid block. It is acknowledged that in reservoir simulation the homogenized fracture–matrix system may lead to imprecise predictions of quantities such as breakthrough times. However, it should be remembered that even if an exact calculation were possible, a precise computation of the breakthrough time would require detailed knowledge of the actual fracture system. Such detailed knowledge is seldom, if ever, available. Consequently, if is felt that, on the average, the homogenized fracture–matrix system will provide meaningful predictions of the important quantities in reservoir simulation.

In Fig. 2 we depict a grid block containing a typical distribution of embedded fractures. The effective permeability for the grid block will be a tensor quantity of the form

$$\mathbb{K} = \begin{pmatrix} \mathrm{K}_{xx} & \mathrm{K}_{xy} & \mathrm{K}_{xz} \\ \mathrm{K}_{yx} & \mathrm{K}_{yy} & \mathrm{K}_{yz} \\ \mathrm{K}_{zx} & \mathrm{K}_{zy} & \mathrm{K}_{zz} \end{pmatrix}. \tag{1}$$

We assume that the effective permeability is the tensor that relates the average fluid velocity, **U**, to the average pressure gradient, **J**, through

$$\mathbf{U} = -\mathbb{K}\mathbf{J}, \tag{2}$$

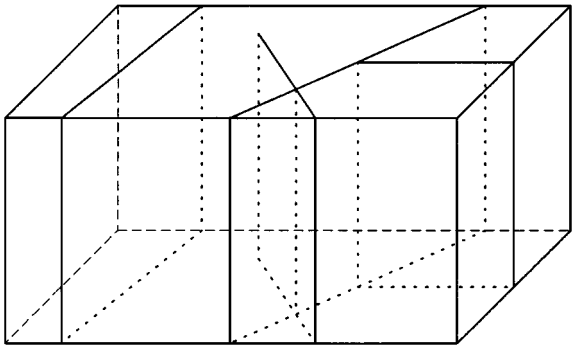

FIG. 2. A grid block may contain several fractures as depicted. These may be randomly oriented, may intersect with one another, and may also terminate inside the grid block.

which is just Darcy's law for the homogenized grid block. The average velocity and pressure gradient are volume averages of the actual velocity and pressure gradient in the grid block. Clearly, if $\mathbf{J} = (1, 0, 0)^T$ then the average velocity is

$$\mathbf{U} = -(\mathrm{K}_{xx}, \mathrm{K}_{yx}, \mathrm{K}_{zx})^T; \tag{3}$$

i.e., the entries in the first column of $\mathbb{K}$ correspond to the components of the average velocity. Similarly, by successively taking the average pressure gradient parallel to the unit vectors $(0, 1, 0)^T$ and $(0, 0, 1)^T$ (and computing the average flow) the remaining two columns of $\mathbb{K}$ can be determined.

Effective permeabilities have been used in other situations to scale-up subgrid permeability heterogeneities (cf. Durlofsky [6]). Periodic-type boundary conditions were used in these instances to compute the fine scale flow through the grid block subject to an imposed average pressure gradient, **J**. The components of the tensor $\mathbb{K}$ were deduced by varying the direction of **J**, computing the resulting average velocity and then employing (2). (As we have already pointed out, the components of $\mathbb{K}$ can be readily deduced by successively choosing **J** to be parallel to each of the three coordinate axes.) This approach for computing effective permeabilities was shown by Bøe [7] to yield a symmetric effective permeability tensor for space filling subgrid heterogeneities. To illustrate what is meant by periodic-type boundary conditions, we need to introduce some notation: suppose S_1 and S_2 are two opposing faces of the grid block and that **x** represents the position vector of an arbitrary point in the grid block. Periodic-type boundary conditions imply that on the surfaces S_1 and S_2 the fluid pressure, p, and its normal velocity, $\mathbf{u} \cdot \mathbf{n}$, satisfy

$$(p - \mathbf{x} \cdot \mathbf{J})|_{S_1} = (p - \mathbf{x} \cdot \mathbf{J})|_{S_2} \tag{5}$$

$$(\mathbf{u} \cdot \mathbf{n})|_{S_1} = -(\mathbf{u} \cdot \mathbf{n})|_{S_2}. \tag{6}$$

In Appendix A, we consider the extension of Bøe's analysis to the situation of a grid block containing subgrid permeability heterogeneities in the form of fractures. We go on to show that this extended analysis implies a symmetric effective grid block permeability tensor for our new modeling approach.

Clearly, the machinery for scaling up subgrid permeability heterogeneities is already quite well established, albeit not for fractures. One of the main ingredients is an approach for computing the fine-scale flow through the heterogeneous grid block. The remainder of this paper is concerned with developing and adapting an efficient model for computing the fine scale flow through fractured grid blocks. In Section 2 we describe the underlying details of this new model, its formulation in terms of a coupled system of boundary integral equations and the solution of that system using the boundary element method. In Section 3 we present some numerical results illustrating different applications of the new flow model, along with some results showing how effective grid block permeabilities can be used in finite difference simulations of fractured reservoirs. Finally, we conclude with a summary of our main results.

2. BOUNDARY INTEGRAL EQUATIONS

In this section we derive the boundary integral equations used in our model. Our main assumption is that the fracture gap is much smaller than any other length scale in the problem. This is a standard assumption when modeling fluid flow through fractures. It permits the

fracture flow to be equated to the two-dimensional flow between a pair of parallel plates as in a Hele–Shaw cell. This, in turn, leads naturally to a system of boundary integral equations (cf., Rasmussen *et al.* [8]). We label these equations as the basic or original system of boundary integral equations and present them in the first subsection that follows. In the second subsection we take further advantage of the small fracture gap size to derive another system of boundary integral equations which is more compact than the original system. It is this new system of equations that forms the core of our model. In our last subsection of this section we describe the boundary element solution procedure for our system of equations. We also describe some steps that we employed to make the solution procedure even more efficient.

2.1. *The Basic Model*

In the basic model the matrix and the fractures are treated as separate systems having a common interface. This common interface is made up of those parts of the fracture boundaries that are contained in the matrix. For the ith fracture, we identify a front planar surface by F_i^+, a back planar surface F_i^- and a lateral boundary F_i^b. It is also convenient to identify the center plane, F_i, in the fracture. This plane is parallel to the front and back surfaces. We will assume that there is a two-dimensional coordinate system for fracture i defined on F_i. If there are N fractures contained in the matrix, the common interface is $\bigcup_{i=1}^{N}(F_i^+ \cup F_i^- \cup F_i^b)$. Together, the matrix and the fracture system occupy a volume V. The part of V occupied by the matrix is denoted by V_m and the part occupied by the ith fracture is denoted by V_i. The gap size for fracture i is denoted by h_i and is the distance between the faces F_i^+ and F_i^-. It is assumed to be much smaller than any other length scale in the problem. The unit normal, $\mathbf{n}_i$, to the central plane F_i is also normal to F_i^+ and F_i^-, and points from F_i^- to F_i^+. (In what follows, the boldface letters $\mathbf{x}$, $\mathbf{y}$, and $\mathbf{z}$ refer to the position vectors of points in V and as such will have three components. Boldface Greek letters, such as $\boldsymbol{\xi}$ and $\boldsymbol{\zeta}$, refer to position vectors of points on one of the fractures, F_i, referenced with respect to the two-dimensional coordinate system on that fracture; i.e., they have only two components.)

Because the fracture gap is small, we assume that for any fracture the flow is equivalent to the flow between a pair of parallel plates. More precisely, the flow in the fracture is assumed to be represented by an average fluid velocity and pressure. This average is over the gap of the fracture so that the average fluid velocity and pressure represents a two-dimensional flow field. (This is the same type of simplification that is adopted in the analysis of flow between infinite parallel plates, as in a Hele–Shaw cell; cf. Homsy [2] for more complete details.) Consequently, if in fracture i the fluid velocity is $\mathbf{u}_i$ and its pressure is p_i then we have

$$\mathbf{u}_i(\boldsymbol{\xi}) = -\kappa_i \bar{\nabla} p_i(\boldsymbol{\xi}) \tag{7a}$$

$$\bar{\nabla} \cdot \mathbf{u}_i(\boldsymbol{\xi}) = -\frac{1}{h_i} Q_i(\boldsymbol{\xi}) + \sum_{j=1}^{m_i} \int_{L_i^j} q_i^j(\boldsymbol{\zeta}) \bar{\delta}(\boldsymbol{\xi} - \boldsymbol{\zeta})\, dl\,(\boldsymbol{\zeta}), \tag{7b}$$

where $Q_i(\boldsymbol{\xi})$ represents the source strength of the fluid flow from fracture i to the matrix. The fractures may intersect with each other, which provides a source or sink for fluid flow at the intersection line. This possibility is accounted for by the line-integral terms appearing on the right-hand side of (7b). It is assumed that there are m_i intersections on fracture i, which are located along the lines $\{L_i^j,\ j = 1, \ldots, m_i\}$ and have corresponding strengths

$\{q_i^j(\boldsymbol{\xi}),\ j=1,\ldots,m_i\}$ (dl represents the line element). The fracture permeability is given by the usual formula for parallel plate flow

$$\kappa_i = h_i^2/12. \tag{8}$$

The differential operator, $\bar{\boldsymbol{\nabla}}$ is the restriction of $\boldsymbol{\nabla}$ to the two-dimensional coordinate system of the fracture and $\bar{\delta}(\cdot)$ is the two-dimensional Dirac delta function. For an individual fracture the boundary is ∂F_i. This either marks the location where the fracture gap size tapers to zero or where the fracture intersects the boundary of the common volume V. In the former case there can be no flow into the matrix at that location, so the appropriate boundary condition is to set the normal flux to zero. In the latter case a normal flux is permitted so the appropriate boundary condition is to set the fracture pressure equal to the pressure on V. (The normal flux in this case depends on the pressure gradient in the fracture, so we need to compute it in the solution process.) Consequently, if ∂V is the boundary of the common volume V, the boundary conditions on the edge of the fracture are

$$\mathbf{n}_i \cdot \mathbf{u}_i(\boldsymbol{\xi}) = 0 \qquad \text{if } \boldsymbol{\xi} \text{ is inside } \partial V \tag{9a}$$

$$p_i(\boldsymbol{\xi}) = p_{\partial V} \quad \text{if } \boldsymbol{\xi} \text{ is on } \partial V, \tag{9b}$$

where $p_{\partial V}$ is the pressure on the boundary ∂V. (As we will see later, when periodic-type boundary conditions are used on ∂V, the boundary condition given by (9a) is used, even though part of ∂F_i may fall on ∂V.)

In the matrix, the fluid is assumed to obey the usual Darcy's law and to be incompressible. Consequently, if the fluid velocity in the matrix is $\mathbf{u}_m$ and its pressure is p_m then we have

$$\mathbf{u}_m(\mathbf{x}) = -\kappa_m \boldsymbol{\nabla} p_m(\mathbf{x}) \tag{10a}$$

$$\boldsymbol{\nabla} \cdot \mathbf{u}_m(\mathbf{x}) = 0, \tag{10b}$$

where κ_m is the matrix permeability. On the external boundary, $\mathbf{u}_m$, p_m, or some combination of $\mathbf{u}_m$ and p_m will be prescribed. The quantity specified generally depends on the problem being solved. On the common interface the pressure is the fracture pressure and the velocity depends on the source strength of the fracture,

$$p_m(\mathbf{x}_i^{\pm}) = p_i(\boldsymbol{\xi}(\mathbf{x}_i^{\pm})) \tag{11a}$$

$$(\mathbf{u}_m(\mathbf{x}_i^{+}) - \mathbf{u}_m(\mathbf{x}_i^{-})) \cdot \mathbf{n}_i = Q_i(\boldsymbol{\xi}(\mathbf{x}_i^{\pm})), \tag{11b}$$

where it is understood that $\mathbf{x}_i^{+}$ and $\mathbf{x}_i^{-}$ are points on the front and back surfaces of the fracture and $\boldsymbol{\xi}(\mathbf{x}_i^{\pm})$ is the corresponding point in the two-dimensional coordinate system of the fracture.

Using Green's identity and the fundamental solution for the two-dimensional Laplacian we readily find the boundary integral equation for the ith fracture,

$$\begin{aligned}\alpha_i p_i(\boldsymbol{\xi}) = &-\int_{\partial F_i} \ln(|\boldsymbol{\zeta}-\boldsymbol{\xi}|)\frac{\partial p_i}{\partial \bar{n}_i}(\boldsymbol{\zeta})\, dl\,(\boldsymbol{\zeta}) + \int_{\partial F_i} \frac{(\boldsymbol{\zeta}-\boldsymbol{\xi})\cdot \bar{\mathbf{n}}_i(\boldsymbol{\zeta})}{|\boldsymbol{\zeta}-\boldsymbol{\xi}|^2} p_i(\boldsymbol{\zeta})\, dl\,(\boldsymbol{\zeta}) \\ &+ \frac{1}{h_i \kappa_i}\int_{F_i} \ln(|\boldsymbol{\zeta}-\boldsymbol{\xi}|)\, Q_i(\boldsymbol{\zeta})\, d\mathcal{A}\,(\boldsymbol{\zeta}) - \frac{1}{\kappa_i}\sum_{j=1}^{n_i}\int_{L_i^j} \ln(|\boldsymbol{\zeta}-\boldsymbol{\xi}|)\, q_i^j(\boldsymbol{\zeta})\, dl\,(\boldsymbol{\zeta}),\end{aligned} \tag{12}$$

where α_i is the angle subtended by ∂F_i at $\boldsymbol{\xi}$ and $d\mathcal{A}$ is the area element. Repeating this procedure for the matrix equations we arrive at the boundary integral equation for the matrix pressure,

$$c_m p_m(\mathbf{x}) = \int_{\partial V} \frac{1}{|\mathbf{y}-\mathbf{x}|} \frac{\partial p_m}{\partial n}(\mathbf{y})\, d\mathcal{A}(\mathbf{y}) + \int_{\partial V} \frac{(\mathbf{y}-\mathbf{x})\cdot\mathbf{n}(\mathbf{y})}{|\mathbf{y}-\mathbf{x}|^3} p_m(\mathbf{y})\, d\mathcal{A}(\mathbf{y}) - \sum_{i=1}^{N} \int_{\partial V_i} \frac{1}{|\mathbf{y}-\mathbf{x}|} \frac{\partial p_m}{\partial n}(\mathbf{y})\, d\mathcal{A}(\mathbf{y}) - \sum_{i=1}^{N} \int_{\partial V_i} \frac{(\mathbf{y}-\mathbf{x})\cdot\mathbf{n}(\mathbf{y})}{|\mathbf{y}-\mathbf{x}|^3} p_m(\mathbf{y})\, d\mathcal{A}(\mathbf{y}), \tag{13}$$

where c_m is the solid angle subtended by the matrix boundary V_m at the point $\mathbf{x}$.

The boundary integral equations given by (12), (13), and the interface conditions (11a) and (11b) are fairly well known. Rasmussen *et al.* [8] used these equations in a boundary element code to compute flow through a rectangular block containing a simple fracture. Accuracy problems were reported for fractures with small gaps, unless a fine mesh was used on the front and back surfaces of the fracture. The fine mesh permitted accurate resolution of differences between the unknowns at the collocation points on the front and back surfaces of the fracture. As we will see in the next section, this problem is circumvented by modeling the fractures as planar sources within the matrix.

2.2. *The New Model*

The fundamental difference between our formulation and the original formulation is that we treat the fractures as planar sources in the matrix. As a result, the matrix and fracture systems are coupled from the outset. The incompressibility relation, for the matrix velocity, which was formerly given by Eq. (10b), becomes

$$\nabla \cdot \mathbf{u}_m(\mathbf{x}) = \sum_{i=1}^{N} \int_{F_i} Q_i(\boldsymbol{\xi}(\mathbf{z}))\, \delta(\mathbf{x}-\mathbf{z})\, d\mathcal{A}(\mathbf{z}), \tag{14}$$

where $\delta(\cdot)$ is the three-dimensional Dirac delta function. Using (14), the boundary integral equation for the matrix pressure (formerly given by (13)) becomes

$$c p_m(\mathbf{x}) = \int_{\partial V} \frac{1}{|\mathbf{y}-\mathbf{x}|} \frac{\partial p_m}{\partial n}(\mathbf{y})\, d\mathcal{A}(\mathbf{y}) + \int_{\partial V} \frac{(\mathbf{y}-\mathbf{x})\cdot\mathbf{n}(\mathbf{y})}{|\mathbf{y}-\mathbf{x}|^3} p_m(\mathbf{y})\, d\mathcal{A}(\mathbf{y}) + \frac{1}{\kappa_m} \sum_{i=1}^{N} \int_{F_i} \frac{1}{|\mathbf{y}-\mathbf{x}|} Q_i(\boldsymbol{\xi}(\mathbf{y}_f))\, d\mathcal{A}(\mathbf{y}), \tag{15}$$

where c is the angle subtended by the boundary of V at $\mathbf{x}$. The system of boundary integral equations given by (12) and (15) is more compact than that given by (12) and (13). The integrals corresponding to the fracture now only comprise single layer potentials. Additionally, there is only one single layer potential type integral for each fracture, as opposed to two for the original formulation (one each for the back and front surfaces). Consequently, the number of integrals required to account for the fractures is reduced by a factor of four by our new formulation. An increase in efficiency of the new approach over the old follows automatically, since a significant portion of the total computation time for the boundary element method is spent evaluating the integrals during equation assembly. Moreover, since

there are fewer unknowns required to describe the fractures, the size of the matrix vector system will be much smaller than for the original formulation. This in turn affects the solution time and has implications for storage requirements. The accuracy of the new equations depends on the difference between Eqs. (13) and (15). In Appendix B we show that (13) can be written as

$$(c_m + c_f)\bar{p}(\mathbf{x}) = \int_{\partial V} \frac{1}{|\mathbf{y}-\mathbf{x}|}\frac{\partial \bar{p}}{\partial n}(\mathbf{y})\, d\mathcal{A}(\mathbf{y}) + \int_{\partial V} \frac{(\mathbf{y}-\mathbf{x})\cdot\mathbf{n}(\mathbf{y})}{|\mathbf{y}-\mathbf{x}|^3}\bar{p}(\mathbf{y})\, d\mathcal{A}(\mathbf{y}) + \frac{1}{\kappa_m}\int_F \frac{1}{|\mathbf{y}_f-\mathbf{x}|} Q(\boldsymbol{\xi}(\mathbf{y}_f))\, d\mathcal{A}(\mathbf{y}_f) + O(h) + O(\kappa_m/\kappa_f), \quad (16)$$

where c_f is the solid angle subtended by the boundary of the fracture (recall that in (13) the fracture is treated as a three-dimensional structure). The "new" pressure term $\bar{p}$ is defined to be the matrix pressure at points in the matrix and the fracture pressure at points inside the fracture. Equation (16) states that (15) is asymptotically equivalent to (13) for small h, i.e., small fracture gap sizes.

Finally, very fine meshes on the fracture are not required since differences between the unknowns on the front and back surfaces of the fracture are "built-into" the new formulation. (Rasmussen *et al.* [8] stated that the separation between mesh points on the front or back surface of the fracture should be less than 10 times the gap size. For the type of problems we intend to investigate the gap size is on the order of 10–100 μm and the "diameter" of a fracture plane is on the order of 1 m. For such a problem, the original formulation would require about 1000×1000 mesh points on the front and back surfaces of the fracture!)

2.3. *Boundary Element Solution of the Model Equations*

In Section 2.2 we showed that the equations describing our model could be very concisely expressed using the boundary integral equations (12) and (15). The boundary conditions on the external boundary have been left quite general up until this point. The boundary conditions depend on the particular type of problem being solved. In the introduction we described how we intended to use this new model for computing effective grid block permeabilities. We also described what was involved in specifying periodic type boundary conditions and that these were the most appropriate boundary conditions to use for computing effective grid block permeabilities. This has implications for the boundary conditions applied at the boundary of a fracture. If a fracture boundary coincides with the grid block boundary, then it should be treated as if the fracture terminates at that location, i.e., the normal velocity is zero and the boundary condition given in (9a) is used on each boundary of the fracture. By imposing such a condition, we can establish a truly periodic system where conditions imposed on opposing faces of the grid block are the same as those expressed in (5) and (6). So now we can state that the system of equations we wish to solve are given by (12) and (15), with boundary conditions for the matrix given by (5) and (6), and boundary conditions for the fracture given by (9a).

When solving this system of equations using the boundary element method, we use rectangular elements on the grid block boundaries or fracture plane surfaces, and linear elements on the fracture edges or fracture intersections. Accordingly, we use either linear or bilinear basis functions to approximate the unknowns. The nodes in the mesh are located at the ends of the linear elements and at the corners of the rectangular elements. At the geometrical corners and edges we permit multiple nodes to occupy the same location, which

helps with the bookkeeping. When collocating the equations we assume the collocation points coincide with the nodal points except at geometrical boundaries and corners. At the geometrical boundaries and corners, the collocation points are moved a certain amount inside their respective elements. This is like what happens in the semi-discontinuous element approach, except in that case the nodal points are also moved away from the geometrical boundaries and corners (cf. Subia *et al.* [9] for a complete description). Our approach neatly circumvents problems with collocating the equations at points corresponding to a double or triple node.

The unknown functions in the formulation are the pressure and normal velocity on the grid block boundary, the pressure and source strength on the fracture planes, the pressure and normal flux on the fracture plane edges, and the line source strengths at the fracture intersections. On account of the periodic boundary conditions, we can identify a single unknown at each point of the grid block boundary. Suppose, for the sake of illustration, that N_1 is a nodal point on one face of the grid block and that the corresponding nodal point on the opposing face of the grid block is N_2. At N_1 we choose the pressure to be the unknown and at N_2 we choose the normal velocity component to be the unknown. The periodic-type boundary conditions imply that the pressure at N_2 can be expressed in terms of the pressure at N_1 and the average pressure gradient. In a similar way the normal velocity component at N_1 can be deduced from that at N_2 and the average pressure gradient. In any case we can define a vector of unknowns, $\mathbf{U}$, where each component represents a value of either the pressure or the normal velocity at each nodal point of the grid block boundary. The vector of unknowns $\mathbf{Q}$ holds the nodal values of the source strength at the nodal points of the fracture planes and the vector of unknowns $\mathbf{p}_f$ holds the nodal values of the pressure. At the nodal points on the fracture plane edges $\mathbf{p}_{fb}$ holds the values of the pressure and $\mathbf{w}_{fb}$ holds the values of the normal component of the velocity. Finally, $\mathbf{q}$ hold the values of the line source strengths at the nodal points on the fracture intersections and $\mathbf{p}_{fi}$ holds the corresponding values of the pressure at the fracture plane intersections.

The matrix vector system resulting from the collocation of our equations has the following block-matrix representation:

$$\begin{pmatrix} \mathrm{A}_1 & \mathrm{B}_1 & 0 & 0 & 0 & 0 \\ \mathrm{A}_2 & \mathrm{B}_2 & \mathrm{C}_2 & 0 & 0 & 0 \\ 0 & \mathrm{B}_3 & \mathrm{C}_3 & \mathrm{D}_3 & \mathrm{E}_3 & \mathrm{F}_3 \\ 0 & 0 & \mathrm{C}_4 & \mathrm{D}_4 & 0 & 0 \\ \mathrm{A}_5 & 0 & 0 & \mathrm{D}_5 & \mathrm{E}_5 & 0 \\ 0 & \mathrm{B}_6 & 0 & \mathrm{D}_6 & \mathrm{E}_6 & \mathrm{F}_6 \end{pmatrix} \begin{pmatrix} \mathbf{U} \\ \mathbf{Q} \\ \mathbf{p}_f \\ \mathbf{p}_{fb} \\ \mathbf{w}_{fb} \\ \mathbf{q} \end{pmatrix} = \begin{pmatrix} \mathbf{R}_1 \\ \mathbf{R}_2 \\ \mathbf{0} \\ \mathbf{0} \\ \mathbf{R}_5 \\ \mathbf{0} \end{pmatrix}. \tag{17}$$

For convenience we have grouped the collocated equations into separate parts or blocks. The first block results from collocating the matrix equations on the grid block boundaries and the second block results from collocating the equations on the fracture plane surfaces. The third block results from collocating the fracture equations on the fracture edges. The fourth block equation simply states that the matrix mesh values of the pressure and fracture mesh values of the pressure must coincide at the fracture edges. The fifth block equation results from explicitly setting boundary conditions at the fracture edges. The sixth block equation results from equating the fracture pressures between each pair of intersecting fractures.

Fortunately, the size of the matrix–vector system in (17) can be reduced significantly. If we choose our unknowns, in $\mathbf{U}$, as $\tilde{p}(\mathbf{x}) = p(\mathbf{x}) - \mathbf{x} \cdot \mathbf{J}$ and $\mathbf{n} \cdot \tilde{\mathbf{u}}_m(\mathbf{x}) = \mathbf{n} \cdot \mathbf{u}_m(\mathbf{x}) + \kappa_m \mathbf{n} \cdot \mathbf{J}$

on the grid block boundary, then it follows that $\mathbf{R}_1 \equiv 0$. Additionally, we note that the block D_4 is just an identity matrix. Furthermore, the block C_2 represents the interpolation of nodal values on the fracture planes at collocation points on the fracture planes. As such, its structure is quite predictable and its inverse, C_2^{-1}, is just as easy to assemble in place of C_2. Periodic boundary conditions requires that we treat all fracture edges as being inside the grid block boundary, from which it follows that $\mathbf{w}_{fb} = \mathbf{0}$. Gathering all these conditions together we can rewrite the matrix–vector system of equations as

$$\begin{pmatrix} A_1 & B_1 & 0 \\ \tilde{A}_3 & \tilde{B}_3 & F_3 \\ \tilde{A}_6 & \tilde{B}_6 & F_6 \end{pmatrix} \begin{pmatrix} \mathbf{U} \\ \mathbf{Q} \\ \mathbf{q} \end{pmatrix} = \begin{pmatrix} \mathbf{0} \\ \mathbf{R}_3 \\ \mathbf{R}_6 \end{pmatrix}, \tag{18}$$

where

$$\begin{aligned} \tilde{A}_3 &= -(C_3 - D_3 C_4) C_2^{-1} A_2 \\ \tilde{A}_6 &= D_6 C_4 C_2^{-1} A_2, \\ \tilde{B}_3 &= B_3 - (C_3 - D_3 C_4) C_2^{-1} B_2 \\ \tilde{B}_6 &= B_6 + D_6 C_4 C_2^{-1} B_2, \\ \mathbf{R}_3 &= -(C_3 - D_3 C_4) C_2^{-1} \mathbf{R}_2 \\ \mathbf{R}_6 &= D_6 C_4 C_2^{-1} \mathbf{R}_2. \end{aligned} \tag{19}$$

Equations (18) and (19) are valid for an arbitrary grid block when periodic boundary conditions are imposed. It is worth noting that if we are processing a number of grid blocks with the same shape, but possibly containing different fracture systems, then it makes sense to compute and store A_1^{-1} and so effect a further reduction in the effective size of the matrix vector system.

3. NUMERICAL EXAMPLES

In this section we present some examples that illustrate our new model for flow in fractured porous media. First, we present a simple example which establishes that the effective permeability calculated in our new model is consistent. We do this by showing that the way the effective permeability changes as the included fracture system is rotated can be predicted theoretically. We go on to present a more complicated example, as might be encountered when analyzing real fracture systems. The increases in efficiency that result from adopting the new model are clearly demonstrated for such an example.

3.1. *Simple Example*

Unfortunately, the periodic boundary conditions required for computing the effective grid block permeabilities leads to equations that are intractable to analytic methods, even for very simple geometries. The example we consider here is of a grid block in the shape of a unit cube containing a single fracture. The fracture has a length of 0.6 units and a gap of 1.0×10^{-4} units. It is vertical and intersects with the top and bottom surfaces of the cube. It is centered at the cube center and is oriented at an angle of θ degrees to the x-direction. The geometry of the cube for a general orientation of the fracture is depicted in Fig. 3. The matrix permeability is set at 1 unit and the fracture permeability is 2.0×10^6 in the same

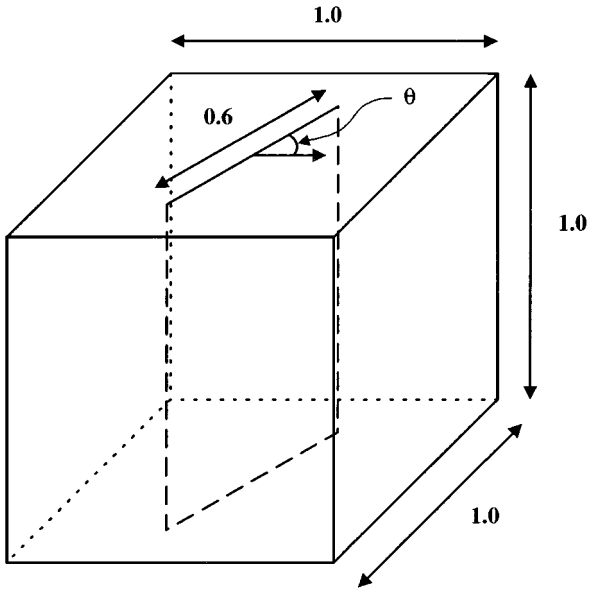

FIG. 3. The geometry of the cube, considered in this example, for a general orientation of the fracture.

units. In computing the effective permeability, a boundary element mesh with seven nodal points for horizontal edges and three nodal points for vertical edges was used.

As we pointed out above, we were unable to find an analytic solution for this simple problem. However, we know that effective grid block permeability will depend on the fracture orientation so that it takes the form

$$\mathbb{K}(\theta) = \begin{pmatrix} \mathrm{K}_{xx}(\theta) & \mathrm{K}_{xy}(\theta) & 0 \\ \mathrm{K}_{yx}(\theta) & \mathrm{K}_{yy}(\theta) & 0 \\ 0 & 0 & \mathrm{K}_{zz}(\theta) \end{pmatrix}. \tag{20}$$

Moreover, if when $\theta = 0$ the effective grid block permeability is

$$\mathbb{K}(0) = \begin{pmatrix} \mathrm{K}_1 & 0 & 0 \\ 0 & \mathrm{K}_2 & 0 \\ 0 & 0 & \mathrm{K}_3 \end{pmatrix}, \tag{21}$$

then it follows that the components given in (20) can be written as

$$\begin{aligned} K_{xx}(\theta) &= K_1 \cos^2\theta + K_2 \sin^2\theta \\ K_{yy}(\theta) &= K_1 \sin^2\theta + K_2 \cos^2\theta \\ K_{zz}(\theta) &= K_3 \\ K_{xy}(\theta) &= K_{yx}(\theta) = (K_1 - K_2)\sin\theta\cos\theta. \end{aligned} \tag{22}$$

The formulae given in (22) provide us with a useful tool for measuring the consistency of the variations in the effective grid block permeability. Using the computed values for K_1, K_2, and K_3 (which are 1.3486, 1.0000, and 2.5951, respectively) we plot the theoretical variation of the effective permeability components in Fig. 4. The values of the components, calculated numerically, are indicated in the plot by unique symbols. Clearly, the numerically

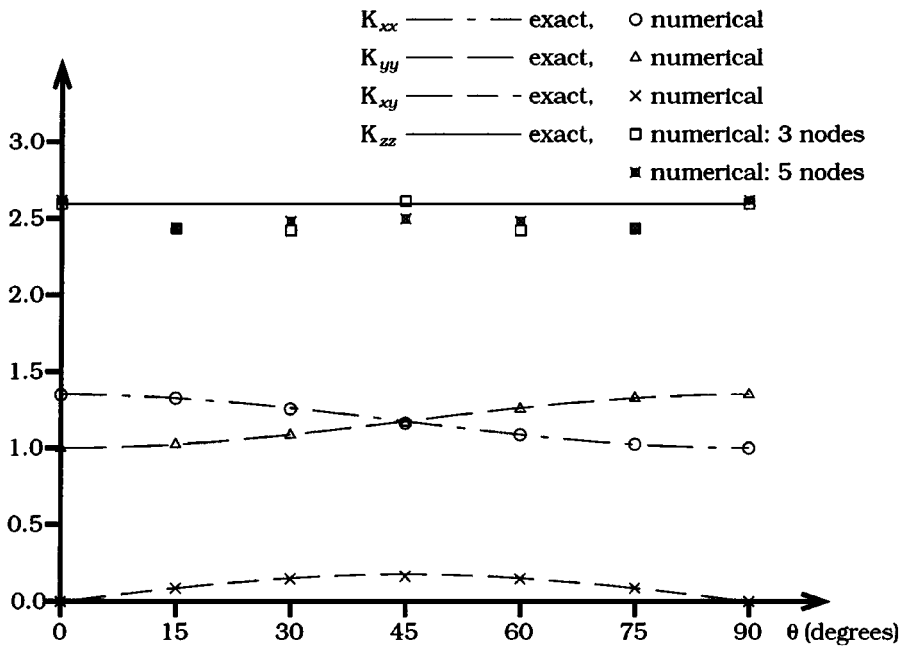

FIG. 4. A plot of the theoretical variation of effective permeability components, for different fracture orientations. The actual numerically computed values are also indicated.

calculated values vary consistently with their theoretically predicted counterparts from (22). Two sets of numerical results are presented for the numerically computed component K_{zz}. As indicated in the plot, the more accurate values were computed using a mesh that had five nodes on the vertical edges, as opposed to the original mesh that had three. The changes in the other components of the permeability tensor are too small to be represented in the plot.

3.2. *Effect of Multiple Fractures on Effective Permeability*

In Section 3.1 we saw that even a grid block containing a single fracture could give rise to a tensorial effective grid block permeability (when the fracture was not aligned with one of the coordinate directions). In this section we illustrate how multiple fractures impact the tensor form of the effective permeability. Starting off with an initial configuration of two fractures in a grid block, we successively add new fractures and show how the tensor form of the effective permeability changes. To simplify the presentation we have chosen to represent the different systems as a 2×2 array of grid blocks as depicted in Fig. 5. The coordinates of the fracture end points are presented in Table 1 for the upper right grid block. The coordinates of the end points of the fractures in the remaining grid are obtained by subtracting (1, 0), (0, 1) or both from the appropriate coordinates in the table. The matrix permeability is set at 1 unit and the fractures are assumed to have uniform permeabilities of $1.0e + 07$ in the same units.

The effective permeabilities for this array of grid blocks is depicted in Fig. 6 for a boundary element mesh that had five nodal points on both horizontal and vertical edges. Repeating the calculation with a boundary element mesh which had seven nodal points on each edge resulted in changes in the principal effective permeabilities that were on the order of only a few percentages. The effective permeability for each grid block is represented by a shaded ellipse; the shade represents the vertical permeability and the ellipse shape captures

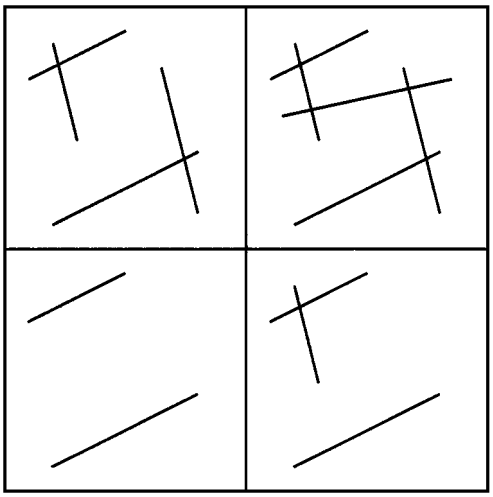

FIG. 5. A 2 × 2 array of naturally fractured grid blocks.

the directional variation of the horizontal permeability, in both magnitude and direction. We see clearly that as each fracture is added the vertical permeability of the grid block increases, which is to be expected. The shape of the horizontal permeability ellipse for the initial configuration is approximately aligned with the two fractures in the grid block. For the next two cases the ellipse changes slightly with the minor axes growing larger. The shape for the final case shows how complicated the interaction of even just five fractures can be.

3.3. *Effective Permeability of Realistic Fracture Systems*

In the previous two subsections we looked at over-simplified examples of fracture systems, which allowed us to illustrate how our new approach works at the grid block level. In practice, we envision our new approach being used to process many fractured grid blocks, with an effective permeability tensor being generated for each grid block. The effective permeability tensors will be use as input for a more traditional simulator, which will permit more realistic simulations of the fractured reservoir.

To illustrate this procedure, we looked at a fracture system generated using statistical data from a naturally fractured, tight gas sand reservoir. The reservoir we chose was in the Mesaverde sandstone in the Piceance Basin (cf. Lorenz and Finley [11]). A tracing of an outcrop of this sandstone is depicted in Fig. 7 (after Lorenz and Finley [11]). Some of the

TABLE 1
The Coordinates of the Fractures in the Upper Right Grid Block of Fig. 5

Fracture coordinates	
(x_1, y_1)	(x_2, y_2)
(1.10, 1.70)	(1.50, 1.90)
(1.20, 1.10)	(1.80, 1.40)
(1.20, 1.85)	(1.30, 1.45)
(1.65, 1.75)	(1.80, 1.15)
(1.15, 1.55)	(1.85, 1.70)

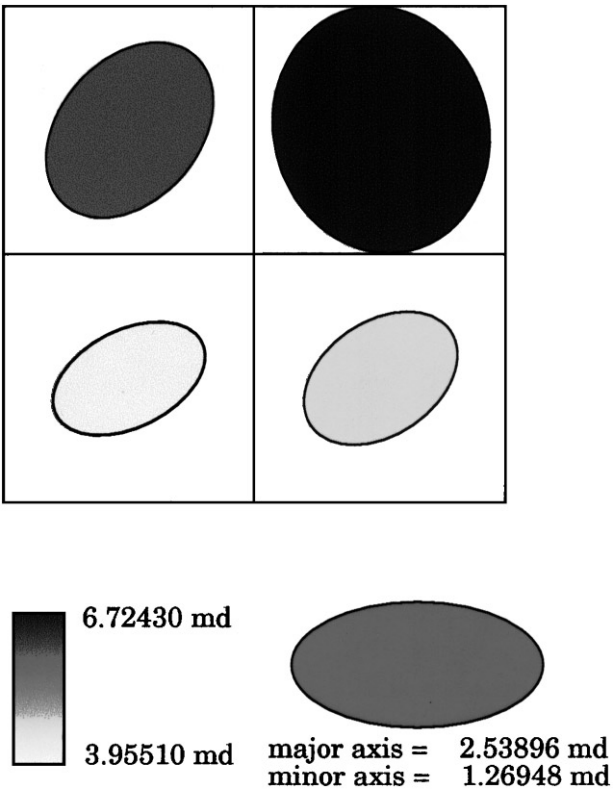

FIG. 6. The effective permeability for the fractured grid blocks in Fig. 5.

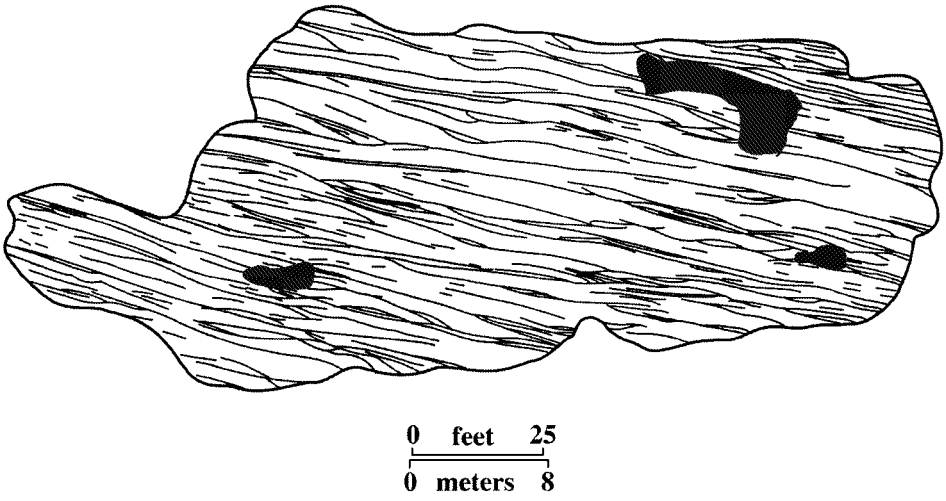

FIG. 7. Tracing of the fractures in an outcrop of the Mesaverde Sandstone at Rifle Gap in the Piceance Basin (after Lorenz and Finley [11]).

TABLE 2
Statistics for the Fractures of the Mesaverde Fracture System as Depicted in Fig. 7

Mesaverde fracture statistics			
Property	Min. value	Max. value	Avg. value
Length (ft)	2.3	108.0	19.2
Orientations (°)	−16	13	4
Intensity (ft/ft^2)	0.48	0.88	0.66

fracture statistics (Lorenz [12]) for this fracture system are presented in Table 2. Additional information was provided regarding the nature of the fracture terminations: 53% of the fractures were found to terminate at no special location; 35% were found to terminate in T-type intersections; 1% were found to terminate at the end of another fracture; and the remainder could not be accounted for because of overlying surface features. Using this data we generated the realization of the fracture system depicted in Fig. 8.

The fractured region measures approximately 70 ft by 210 ft. We subdivided the region uniformly into a grid of 15 by 30 cells. In our boundary element code, we computed the effective permeability tensor for each grid block assuming a matrix permeability of 2 md and a uniform fracture aperture of 100 μm. We used this permeability information in a finite difference code to examine flow through the system. This code was based on a flux continuous finite difference scheme (cf. Edwards and Rogers [13]) so that we could effectively use the full tensor information available for each grid block. We also assumed that the top and bottom boundaries of this fractured region were no-flow boundaries. To establish flow through the region, we applied an average unit pressure gradient in the negative x direction by requiring a specific pressure difference between the opposing ends of the region. Using this configuration, we computed the corresponding steady state flow.

Figure 9 shows the impact of variations in the effective permeability on the motion of the fluid through the region. The fluid at the right-hand side of the region was marked with a tracer at a certain point in time. Three snapshots of the subsequent evolution of the tracer are presented in the figure. They help to illustrate how fluid moves through the homogenized grid blocks. In the bottom plot of the figure we see that the variations in the effective permeability have had a pronounced and cumulative effect on the flow through

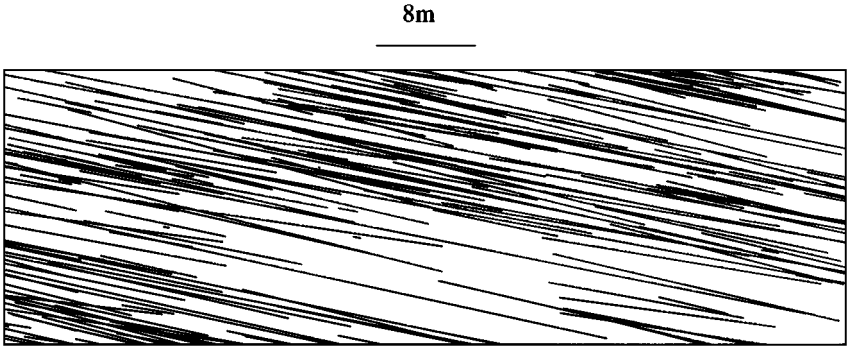

FIG. 8. Fracture realization generated using statistics from the Mesaverde fracture system presented in Table 2.

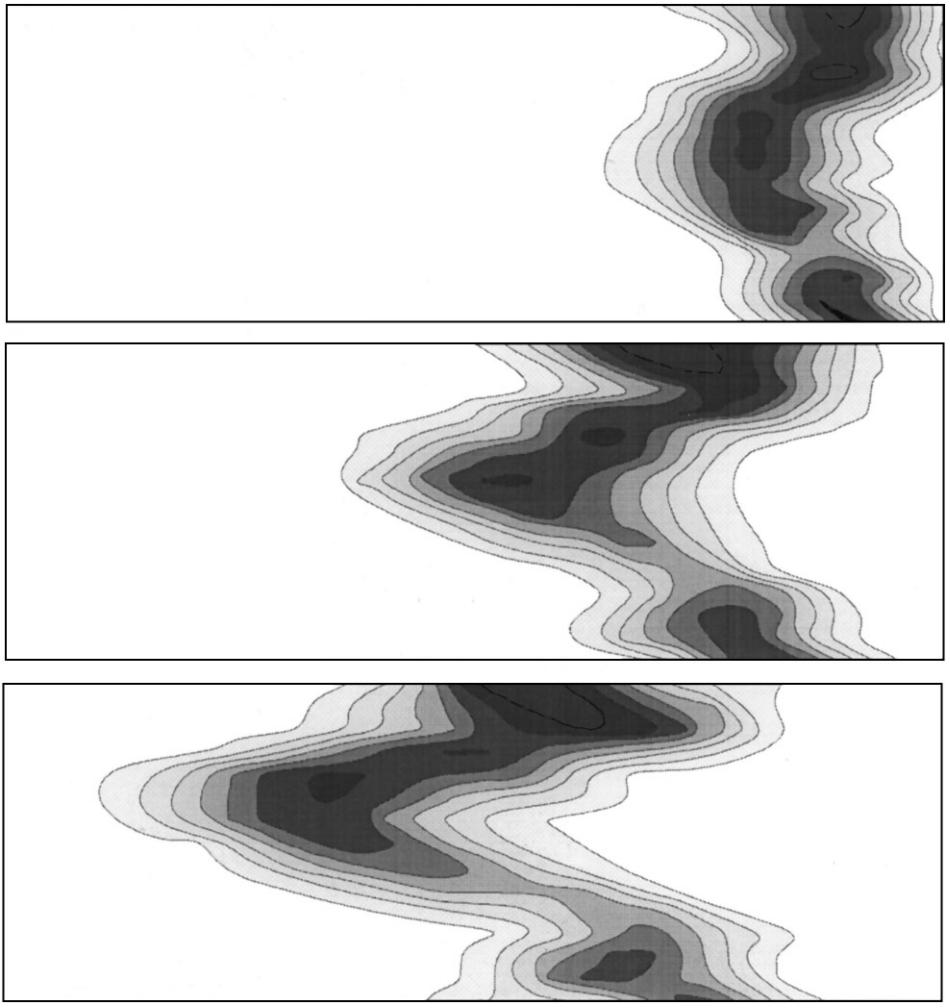

FIG. 9. Three successive snapshots of the evolution of a tracer through the fracture system depicted in Fig. 8. The motion of the tracer through the homogenized grid blocks illustrates the general motion of the fluid.

the region. By comparing the concentrations of the tracer, with the fractures in Fig. 8, we see that the tracer flow, and consequently the fluid flow, is primarily determined by the orientation and intensity of fracturing. Clearly, the directional permeability information, originally contained in the fracture system, is now contained in the effective permeability values of the homogenized grid block.

4. CONCLUSIONS

In this paper we have introduced a new approach for computing fluid flow through fractured porous media. The model is based on the treatment of fractures as special source planes in the matrix and the resulting equations are solved using the boundary element method. The equations in our new model are asymptotically equivalent to a more traditional model which treats the fractures as rectangular voids. However, in contrast to the more traditional model, the results from our new model are insensitive to the ratio of the fracture

node spacing to void gap. Additionally, our new method can boast of increases in efficiency resulting from fewer nodes and fewer integral evaluations.

As a practical application, we related the fluid flow results of our new model to the effective permeability of rectangular grids blocks. Furthermore, we showed that this grid block permeability tensor was symmetric if periodic-type boundary conditions were used in the boundary integral equations. In the boundary element implementation, we showed how the full solution could be obtained by solving a significantly smaller system of equations. In the examples section, we presented a numerical example that demonstrated that the effective permeability tensor was being consistently calculated and a second example that showed how fracture-matrix interactions, as well as fracture–fracture interactions, were impacting the effective permeability tensor.

APPENDIX A: SYMMETRY OF THE EFFECTIVE GRID BLOCK PERMEABILITY

In Section 1, we pointed out that the effective grid block permeability satisfies the homogenized form of Darcy's equation, so that if $\mathbf{J}$ is the average pressure gradient in the grid block, then the average velocity is given by

$$\mathbf{U} = -\mathbb{K}\mathbf{J}. \tag{A1}$$

We can identify three fundamental average pressure gradients

$$\left\{\mathbf{J}^{(1)}, \mathbf{J}^{(2)}, \mathbf{J}^{(3)}\right\} = \left\{ \begin{pmatrix} 1 \\ 0 \\ 0 \end{pmatrix}, \begin{pmatrix} 0 \\ 1 \\ 0 \end{pmatrix}, \begin{pmatrix} 0 \\ 0 \\ 1 \end{pmatrix} \right\}, \tag{A2}$$

so that a linear combination of these will admit any average pressure gradient. Corresponding to the fundamental pressure gradients, there are three average velocities

$$\left\{\mathbf{U}^{(1)}, \mathbf{U}^{(2)}, \mathbf{U}^{(3)}\right\} = \left\{ \begin{pmatrix} \mathrm{K}_{11} \\ \mathrm{K}_{21} \\ \mathrm{K}_{31} \end{pmatrix}, \begin{pmatrix} \mathrm{K}_{12} \\ \mathrm{K}_{22} \\ \mathrm{K}_{32} \end{pmatrix}, \begin{pmatrix} \mathrm{K}_{13} \\ \mathrm{K}_{23} \\ \mathrm{K}_{33} \end{pmatrix} \right\}, \tag{A3}$$

where we have used numerical subscripts to refer to the components of $\mathbb{K}$. Clearly, we can write

$$\begin{aligned} K_{ij} &= \mathbf{J}^{(i)} \cdot \left(\mathbb{K}\mathbf{J}^{(j)}\right) \\ &= -\mathbf{J}^{(i)} \cdot \mathbf{U}^{(j)} \\ &= -\frac{1}{|V|}\mathbf{J}^{(i)} \cdot \int_V \mathbf{u}^{(j)}\, d\mathcal{V}, \end{aligned} \tag{A4}$$

where V is the grid block and $|V|$ is its volume.

Bøe [7] showed that if the grid block was composed of two regions, V_1 and V_2, which have tensor permeabilities of $\mathbb{K}_1$ and $\mathbb{K}_2$, respectively, then the components of the effective grid block permeability are given by

$$K_{ij} = \frac{1}{|V|}\int_{V_1} \boldsymbol{\nabla} p^{(i)} \cdot \left(\mathbb{K}_1 \boldsymbol{\nabla} p^{(j)}\right) d\mathcal{V} + \frac{1}{|V|}\int_{V_2} \boldsymbol{\nabla} p^{(i)} \cdot \left(\mathbb{K}_2 \boldsymbol{\nabla} p^{(j)}\right) d\mathcal{V}, \tag{A5}$$

which is symmetric whenever the local permeabilities are symmetric. The crucial relation,

required to establish (A5), is that

$$\int_{\partial V} p^{(i)}\mathbf{n}\cdot\mathbf{u}^{(j)}\,d\mathcal{A} = \int_{\partial V} P^{(i)}\mathbf{n}\cdot\mathbf{u}^{(j)}\,d\mathcal{A}, \tag{A6}$$

where $P^{(i)} = \mathbf{x}\cdot\mathbf{J}^{(i)}$ is the linear pressure profile with constant gradient given by $\mathbf{J}^{(i)}$. Equation (A6) is a direct result of the periodic boundary conditions satisfied by $p^{(i)}$ and $\mathbf{u}^{(i)}$.

Unfortunately, when the grid block is composed of a matrix region and a fracture region, (A5) cannot be used directly to express the components of the effective grid block permeability, although the relationship expressed in (A6) is still valid. The main reason is that the fracture permeability, $\mathbb{K}_f$, is a two-dimensional tensor, which corresponds to the fact that the fracture is effectively two-dimensional. The most convenient way of establishing the correct formula for the components of $\mathbb{K}$ is to assume that the fracture occupies a region of thickness ϵ centered on the fracture plane F. We will refer to the corresponding volume as V_f. This necessitates that the matrix occupies the volume $V_m = V - V_f$. To preserve the correct flux through the fracture we redefine the fracture velocity to be $h\mathbf{u}_f/\epsilon$. Note that h is the actual fracture gap size. After we perform some manipulations on the components of $\mathbb{K}$ we can let $\epsilon \to 0$ to get the correct expression for the components of $\mathbb{K}$. Using (A4) we find

$$\begin{aligned}
K_{ij} &= -\frac{\mathbf{J}^{(i)}}{|V|}\cdot\left(\int_{V_m}\mathbf{u}_m^{(j)}\,d\mathcal{V} + \frac{h}{\epsilon}\int_{V_f}\mathbf{u}_f^{(j)}\,d\mathcal{V}\right)\\
&= -\frac{1}{|V|}\left(\int_{V_m}\mathbf{J}^{(i)}\cdot\mathbf{u}_m^{(j)}\,d\mathcal{V} + h\int_F \mathbf{J}^{(i)}\cdot\mathbf{u}_f^{(j)}\,d\mathcal{A}\right)\\
&= -\frac{1}{|V|}\left(\int_{\partial V} P^{(i)}\mathbf{n}\cdot\mathbf{u}_m^{(j)}\,d\mathcal{A} - \int_{\partial V_f} P^{(i)}\mathbf{n}\cdot\mathbf{u}_m^{(j)}\,d\mathcal{A} + \int_F P^{(i)}Q^{(j)}\,d\mathcal{A}\right)\\
&= -\frac{1}{|V|}\left(\int_{\partial V_m} p^{(i)}\mathbf{n}\cdot\mathbf{u}_m^{(j)}\,d\mathcal{A} - \int_{\partial V_f}\left(P^{(i)}-p^{(i)}\right)\mathbf{n}\cdot\mathbf{u}_m^{(j)}\,d\mathcal{A} + \int_F P^{(i)}Q^{(j)}\,d\mathcal{A}\right)\\
&= -\frac{1}{|V|}\left(\int_{V_m}\nabla p^{(i)}\cdot\mathbf{u}_m^{(j)}\,d\mathcal{V}\right)\\
&\quad + \frac{1}{|V|}\left(\frac{\epsilon\mathbf{n}_f\cdot\mathbf{J}^{(i)}}{2}\int_F \mathbf{n}_f\cdot\left(\mathbf{u}_m^{(j)}\big|_{F^+} + \mathbf{u}_m^{(j)}\big|_{F^-}\right)d\mathcal{A} - \int_F p^{(i)}Q^{(j)}\,d\mathcal{A}\right)\\
&= \frac{1}{|V|}\left(\int_{V_m}\nabla p^{(i)}\cdot\left(\mathbb{K}_m\nabla p^{(j)}\right)d\mathcal{V} + h\int_F \bar{\nabla}p^{(i)}\cdot\left(\mathbb{K}_f\bar{\nabla}p^{(j)}\right)d\mathcal{A}\right)\\
&\quad + \frac{\epsilon\mathbf{n}_f\cdot\mathbf{J}^{(i)}}{2|V|}\int_F \mathbf{n}_f\cdot\left(\mathbf{u}_m^{(j)}\big|_{F^+} + \mathbf{u}_m^{(j)}\big|_{F^-}\right)d\mathcal{A}.
\end{aligned}\tag{A7}$$

In deriving (A7) we used (A6) along with the following observations:

(1) u_f is based on a two-dimensional velocity field with no component or variation perpendicular to F,

(2) the average pressure is $P^{(i)} = \mathbf{x}\cdot\mathbf{J}^{(i)}$, which implies that

$$\left[P^{(i)}\mathbf{n}_f\mathbf{u}_m^{(j)}\right]_{F^\pm} = \left(P_F^{(i)} \pm \left(\frac{\epsilon}{2}\right)\mathbf{n}_f\cdot\mathbf{J}^{(i)}\right)\left(\mathbf{n}_f\cdot\mathbf{u}_m^{(j)}\big|_{F^\pm}\right), \tag{A8}$$

(3) the source strength is $Q^{(j)} = [\mathbf{n}_f\cdot\mathbf{u}_m^{(j)}]_{F^-}^{F^+}$.

At this point we should remark that (A7) gives the formula for the components of the effective grid block permeability for the basic or original model if ϵ is replaced by h. In general, $\mathbb{K}$ will not be symmetric in this case. However, to get the result corresponding to our new model, we let $\epsilon \to 0$ to find

$$K_{ij} = \frac{1}{|V|}\left(\int_V \boldsymbol{\nabla} p^{(i)} \cdot \left(\mathbb{K}_m \boldsymbol{\nabla} p^{(j)}\right) d\mathcal{V} + h \int_F \bar{\boldsymbol{\nabla}} p^{(i)} \cdot \left(\mathbb{K}_f \bar{\boldsymbol{\nabla}} p^{(j)}\right) d\mathcal{A} \right) \quad \text{(A9)}$$

which is symmetric so long as $\mathbb{K}_m$ and $\mathbb{K}_f$ are both symmetric.

APPENDIX B: ASYMPTOTIC FORM OF THE BASIC MODEL FOR SMALL GAP SIZE

In this appendix we show that the new formulation for the matrix pressure, Eq. (15), is asymptotically equivalent to that in the basic model, Eq. (13), for small fracture gap size. For simplicity, assume that we have a single fracture of thickness h occupying a volume V_f in a porous matrix. As in Section 2.1 we identify three planar surfaces with the fracture: a front surface F^+, a central plane F, and a back surface F^-. The lateral boundary of the fracture is denoted by F^b. The unit fracture normal $\mathbf{n}_f$ is orthogonal to F and points from F^- to F^+. Although we use a two-dimensional coordinate system attached to F, to label points on the fracture we will also assume that $\mathbf{x}_f$ refers to a point on F in terms of the three-dimensional coordinate system of the matrix. Consequently, at the point $\boldsymbol{\xi}(\mathbf{x}_f)$ the fracture source strength is

$$\begin{aligned} Q(\boldsymbol{\xi}(\mathbf{x}_f)) &= \left(\mathbf{u}_m\left(\mathbf{x}_f + \frac{h}{2}\mathbf{n}_f\right) - \mathbf{u}_m\left(\mathbf{x}_f - \frac{h}{2}\mathbf{n}_f\right)\right) \cdot \mathbf{n}_f \\ &= -\kappa_m \left(\frac{\partial p_m}{\partial n_f}\left(\mathbf{x}_f + \frac{h}{2}\mathbf{n}_f\right) - \frac{\partial p_m}{\partial n_f}\left(\mathbf{x}_f - \frac{h}{2}\mathbf{n}_f\right)\right). \end{aligned} \quad \text{(B1)}$$

We will use this expression in what follows. We also define an auxiliary function $\bar{p}(\mathbf{x})$ in terms of the fracture pressure

$$\bar{p}(\mathbf{x}_f + \eta \mathbf{n}_f) = p_f(\boldsymbol{\xi}(\mathbf{x}_f)), \quad \text{(B2)}$$

where $\mathbf{x}_f$ lies on the central plane, F, in the fracture and $-h/2 < \eta < h/2$. It is worth stressing, at this point, that $\boldsymbol{\xi}(\mathbf{x}_f)$ is the projection of $\mathbf{x}_f + \eta\mathbf{n}_f$ onto the two-dimensional coordinate system of the central plane. The auxiliary pressure is really the fracture pressure as a function of position in the three-dimensional coordinate system of the matrix. We can take the three-dimensional Laplacian of $\bar{p}$, to find that inside the fracture volume we have

$$\begin{aligned} \nabla^2 \bar{p}(\mathbf{x}_f + \eta\mathbf{n}_f) &= \bar{\nabla}^2 p_f(\boldsymbol{\xi}(\mathbf{x}_f)) \\ &= \frac{1}{h\kappa_f} Q(\boldsymbol{\xi}(\mathbf{x}_f)) \end{aligned} \quad \text{(B3)}$$

which is a direct consequence of (7a) and (7b). Using Green's identity, the fundamental solution for the three-dimensional Laplacian and the boundary conditions, we find that the

auxiliary pressure satisfies

$$c_f \bar{p}(\mathbf{x}) = \int_{\partial V_f} \frac{(\mathbf{y}-\mathbf{x})\cdot\mathbf{n}(\mathbf{y})}{|\mathbf{y}-\mathbf{x}|^3} p_m(\mathbf{y})\, d\mathcal{A}(\mathbf{y}) - \frac{1}{h\kappa_f}\int_{V_f} \frac{1}{|\mathbf{y}-\mathbf{x}|} Q(\boldsymbol{\xi}(\mathbf{y}))\, d\mathcal{V}(\mathbf{y}), \quad \text{(B4)}$$

where $d\mathcal{V}$ is the volume element.

Now we consider the reduction of (13), which we restate for the sake of continuity:

$$\begin{aligned} c_m p_m(\mathbf{x}) = &\int_{\partial V} \frac{1}{|\mathbf{y}-\mathbf{x}|}\frac{\partial p_m}{\partial n}(\mathbf{y})\, d\mathcal{A}(\mathbf{y}) + \int_{\partial V} \frac{(\mathbf{y}-\mathbf{x})\cdot\mathbf{n}(\mathbf{y})}{|\mathbf{y}-\mathbf{x}|^3} p_m(\mathbf{y})\, d\mathcal{A}(\mathbf{y}) \\ &- \int_{\partial V_f} \frac{1}{|\mathbf{y}-\mathbf{x}|}\frac{\partial p_m}{\partial n}(\mathbf{y})\, d\mathcal{A}(\mathbf{y}) - \int_{\partial V_f} \frac{(\mathbf{y}-\mathbf{x})\cdot\mathbf{n}(\mathbf{y})}{|\mathbf{y}-\mathbf{x}|^3} p_m(\mathbf{y})\, d\mathcal{A}(\mathbf{y}). \quad \text{(B5)} \end{aligned}$$

We immediately see that, according to (B4), the last integral in (B5) can be expressed in terms of the auxiliary pressure and the source strength. A relation for the second last integral in (B5) follows by using the definition of the source strength:

$$\begin{aligned} &\int_{\partial V_f} \frac{1}{|\mathbf{y}-\mathbf{x}|}\frac{\partial p_m}{\partial n}(\mathbf{y})\, d\mathcal{A}(\mathbf{y}) \\ &\quad = + \int_F \left[\frac{1}{|\mathbf{y}_f - \mathbf{x} + (h/2)\mathbf{n}_f|} - \frac{1}{|\mathbf{y}_f - \mathbf{x}|}\right]\frac{\partial p_m}{\partial n_f}\left(\mathbf{y}_f + \frac{h}{2}\mathbf{n}_f\right) d\mathcal{A}(\mathbf{y}_f) \\ &\qquad - \int_F \left[\frac{1}{|\mathbf{y}_f - \mathbf{x} - (h/2)\mathbf{n}_f|} - \frac{1}{|\mathbf{y}_f - \mathbf{x}|}\right]\frac{\partial p_m}{\partial n_f}\left(\mathbf{y}_f - \frac{h}{2}\mathbf{n}_f\right) d\mathcal{A}(\mathbf{y}_f) \\ &\qquad - \frac{1}{\kappa_m}\int_F \frac{1}{|\mathbf{y}_f - \mathbf{x}|} Q(\boldsymbol{\xi}(\mathbf{y}_f))\, d\mathcal{A}(\mathbf{y}_f). \quad \text{(B6)} \end{aligned}$$

We will now show that the second integral on the right-hand side of (B4) and the first two integrals on the right-hand side of (B6) are either $O(h)$ or $O(\kappa_m/\kappa_f)$. To see this we make the simple observation that for any $\mathbf{x}$ we have

$$\begin{aligned} \left|\int_F \frac{1}{|\mathbf{y}_f - \mathbf{x}|}\, d\mathcal{A}(\mathbf{y}_f)\right| &\le \max_{\mathbf{x}_f \in F} \int_F \frac{1}{|\mathbf{y}_f - \mathbf{x}_f + \eta\mathbf{n}_f|}\, d\mathcal{A}(\mathbf{y}_f) \\ &\le \int_0^R \int_0^{2\pi} \frac{r\, dr\, d\theta}{\sqrt{r^2+\eta^2}} \\ &\le 2\pi\left(\sqrt{R^2+\eta^2} - \eta\right) \\ &\le 2\pi R, \quad \text{(B7)} \end{aligned}$$

where (r, θ) are polar coordinates centered at $\mathbf{x}_f$, R is the radius of the smallest circle (again centered at $\mathbf{x}_f$) that contains F, and η is the perpendicular distance of $\mathbf{x}$ from F. Using (B7) we find

$$\left|\int_{V_f} \frac{1}{|\mathbf{y}-\mathbf{x}|} Q(\boldsymbol{\xi}(\mathbf{y}))\, d\mathcal{V}(\mathbf{y})\right| \le 2\pi h R\left(\max_{\mathbf{x}_f \in F}\left|Q(\boldsymbol{\xi}(\mathbf{x}_f))\right|\right). \quad \text{(B8)}$$

We also have

$$\left|\int_F \left[\frac{1}{|\mathbf{y}_f - \mathbf{x} \pm (h/2)\mathbf{n}_f|} - \frac{1}{|\mathbf{y}_f - \mathbf{x}|}\right] d\mathcal{A}(\mathbf{y}_f)\right| = \frac{h}{2}\left|\int_F \frac{\mathbf{n}_f \cdot (\mathbf{y}_f - \mathbf{x} + \epsilon_\pm \mathbf{n}_f)}{|\mathbf{y}_f - \mathbf{x} + \epsilon_\pm \mathbf{n}_f|^3} d\mathcal{A}(\mathbf{y}_f)\right| \leq 2\pi h, \tag{B9}$$

where $\epsilon_\pm \in [-h/2, h/2]$ depends on $\mathbf{x}$ and $\mathbf{y}_f$. In (B9), the transformation from the integral term to the term on the right-hand side of the inequality follows by realizing that the integral is the solid angle ($\leq 4\pi$) subtended at $\mathbf{x}$ by a surface. This surface is that which results from a nonuniform distortion of F. The amount of distortion at any point of F is given by $\epsilon_\pm$, which generally is nonuniform. Using (B9) we find

$$\left|\int_F \left[\frac{1}{|\mathbf{y}_f - \mathbf{x} + (h/2)\mathbf{n}_f|} - \frac{1}{|\mathbf{y}_f - \mathbf{x}|}\right] \frac{\partial p_m}{\partial n_f}\left(\mathbf{y}_f + \frac{h}{2}\mathbf{n}_f\right) d\mathcal{A}(\mathbf{y}_f)\right| \leq 2\pi h\left(\max_{\mathbf{x}_f \in F}\left|\frac{\partial p_m}{\partial n_f}\left(\mathbf{x}_f + \frac{h}{2}\mathbf{n}_f\right)\right|\right) \tag{B10}$$

and

$$\left|\int_F \left[\frac{1}{|\mathbf{y}_f - \mathbf{x} - (h/2)\mathbf{n}_f|} - \frac{1}{|\mathbf{y}_f - \mathbf{x}|}\right] \frac{\partial p_m}{\partial n_f}\left(\mathbf{y}_f - \frac{h}{2}\mathbf{n}_f\right) d\mathcal{A}(\mathbf{y}_f)\right| \leq 2\pi h\left(\max_{\mathbf{x}_f \in F}\left|\frac{\partial p_m}{\partial n_f}\left(\mathbf{x}_f - \frac{h}{2}\mathbf{n}_f\right)\right|\right). \tag{B11}$$

Using (B8) in (B4) and both (B10) and (B11) in (B6), we can rewrite (B5) as

$$c_m p_m(\mathbf{x}) = \int_{\partial V} \frac{1}{|\mathbf{y} - \mathbf{x}|}\frac{\partial p_m}{\partial n}(\mathbf{y})\, d\mathcal{A}(\mathbf{y}) + \int_{\partial V} \frac{(\mathbf{y} - \mathbf{x}) \cdot \mathbf{n}(\mathbf{y})}{|\mathbf{y} - \mathbf{x}|^3} p_m(\mathbf{y})\, d\mathcal{A}(\mathbf{y}) + \frac{1}{\kappa_m}\int_F \frac{1}{|\mathbf{y}_f - \mathbf{x}|} Q(\boldsymbol{\xi}(\mathbf{y}_f))\, d\mathcal{A}(\mathbf{y}_f) + O(h) - c_f \bar{p}(\mathbf{x}) + O(\kappa_m/\kappa_f). \tag{B12}$$

Finally, we extend the auxiliary pressure outside the fracture so that it coincides with the matrix pressure

$$\bar{p}(\mathbf{x}) = p_m(\mathbf{x}) \tag{B13}$$

for $\mathbf{x}$ in V_m. Using the auxiliary pressure we can write

$$(c_m + c_f)\bar{p}(\mathbf{x}) = \int_{\partial V} \frac{1}{|\mathbf{y} - \mathbf{x}|}\frac{\partial \bar{p}}{\partial n}(\mathbf{y})\, d\mathcal{A}(\mathbf{y}) + \int_{\partial V} \frac{(\mathbf{y} - \mathbf{x}) \cdot \mathbf{n}(\mathbf{y})}{|\mathbf{y} - \mathbf{x}|^3} \bar{p}(\mathbf{y})\, d\mathcal{A}(\mathbf{y}) + \frac{1}{\kappa_m}\int_F \frac{1}{|\mathbf{y}_f - \mathbf{x}|} Q(\boldsymbol{\xi}(\mathbf{y}_f))\, d\mathcal{A}(\mathbf{y}_f) + O(h) + O(\kappa_m/\kappa_f). \tag{B14}$$

Besides the $O(h)$ and $O(\kappa_m/\kappa_f)$ terms, the only other difference between (B14) and (15) is the solid angle term that multiplies the pressure on the left-hand side of both equations. However, $c_m + c_f$ is the solid angle subtended at $\mathbf{x}$ by ∂V, i.e., $c_m + c_f = c$. In other

words, (B14) and (15) are the same equation, up to terms of order $O(h)$ and $O(\kappa_m/\kappa_f)$. Since (B14) is the transformed version of (B5) it is also the transformed version of (13). Consequently, we can conclude that Eq. (15) is the leading order term in an asymptotic expansion of Eq. (13) for small h.

ACKNOWLEDGMENTS

The work presented in this paper was supported jointly by the Strategic Research Department at Chevron Petroleum Technology Company and by the Gas Research Institute Contract 5094-210-3050.

REFERENCES

1. J. Bear, *Dynamics of Fluids in Porous Media* (Elsevier, New York, 1972).
2. G. M. Homsy, Viscous fingering in porous media, *Annu. Rev. Fluid Mech.* **19**, 271 (1987).
3. J. P. Chiles, Three-dimensional geometric modeling of a fracture network, *Proceedings of the Conference on Geostatistical, Sensitivity, and Uncertainty Methods for Ground-Water Flow and Radionuclide Transport Modeling, San Francisco, California, September 1987*, edited by B. E. Buxton (Battelle Press, Columbus, OH, 1987), p. 361.
4. S. E. Laubach, Fracture patterns in low permeability sandstone gas reservoir rocks in the Rocky Mountain region, at *Rocky Mountain Regional Meeting and Low Permeability Reservoirs Symposium, April 1991, Denver*, Paper SPE 21853.
5. J. C. Lorenz and R. E. Hill, Subsurface fracture spacing: Comparison of inferences from slant/horizontal core and vertical core in Mesaverde Reservoirs, presented at *Rocky Mountain Regional Meeting and Low Permeability Reservoirs Symposium, April 1991, Denver*, Paper SPE 21877.
6. L. J. Durlofsky, Numerical calculation of equivalent grid block permeability tensors for heterogeneous porous media, *Water Resources Research*, **27**, 699 (1991).
7. Ø. Bøe, Analysis of an upscaling method based on conservation of dissipation, *Transport Porous Media* **17**, 77 (1994).
8. T. C. Rasmussen, T. C. J. Yeh, and D. D. Evans, Effect of variable fracture permeability/matrix permeability ratios on three-dimensional fractured rock hydraulic conductivity, *Proceedings of the Conference on Geostatistical, Sensitivity, and Uncertainty Methods for Ground-Water Flow and Radionuclide Transport Modeling, San Francisco, California, September 1987*, edited by B. E. Buxton (Batelle Press, Columbus, OH, 1987), p. 337.
9. S. R. Subia, M. S. Ingber, and A. K. Mitra, A comparison of the semidiscontinuous element and multiple node with auxiliary Boundary Collocation Approaches for the boundary element method. *Engineering Analysis with Boundary Elements* **15**, 19 (1995).
10. C. A. Brebbia, *The Boundary Element Method for Engineers* (Pentech, London, 1978).
11. J. C. Lorenz and S. J. Finley, Regional fractures II: Fracturing of Mesaverde Reservoirs in the Piceance Basin, Colorado, *Bull. AAPG* **75**(11), 1738 (1991).
12. J. C. Lorenz, private communication.
13. M. G. Edwards and C. F. Rogers, A flux continuous finite difference scheme for the full tensor pressure equation, in *ECMOR IV, 4th European Conference on the Mathematics of Oil Recovery, Røros, Norway, 1994.*